RSC Advances

PAPER

View Article Online
View Journal | View Issue

Cite this: *RSC Adv.*, 2019, **9**, 7903

TiO_2-coated $LiCoO_2$ electrodes fabricated by a sputtering deposition method for lithium-ion batteries with enhanced electrochemical performance†

Sang-Hyun Moon, Min-Cheol Kim, Eun-Soo Kim, Yeon-Kyung Shin, Ji-Eun Lee, Sojeong Choi and Kyung-Won Park *

We fabricated lithium cobalt oxide ($LiCoO_2$, LCO) electrodes in the absence and presence of TiO_2 layers as cathodes for lithium-ion batteries (LIBs) using a sputtering deposition method under an Ar atmosphere. In particular, TiO_2 coating layers on sputtered LCO electrodes were directly deposited in a layer-by-layer form with varying TiO_2 sputtering times from 60 to 120 s. These sputtered electrodes were heated at 600 °C in an air atmosphere for 3 h. The thicknesses of TiO_2 layers in TiO_2-coated LCO electrodes were controlled from ~2 to ~10 nm. These TiO_2-coated LCO electrodes exhibited superior electrochemical performance, *i.e.* high capacities (93–107 mA h g^{-1}@0.5C), improved retention of >60% after 100 cycles, and high-rate cycling properties (64 mA h g^{-1}@1C after 100 cycles). Such an improved performance of TiO_2-coated LCO electrodes was found to be attributed to relieved volumetric expansion of LCO and protection of LCO electrodes against HF generated during cycling.

Received 20th December 2018
Accepted 4th March 2019

DOI: 10.1039/c8ra10451d

rsc.li/rsc-advances

1 Introduction

Li-ion batteries (LIBs) are attractive as electrochemical power sources for portable electronic devices and electric vehicles due to their high energy densities and long cycle life.[1–5] Recently, thin-film technologies that can fabricate small-sized LIBs for drones and medical devices have been reported.[6–8] In particular, lithium cobalt oxide ($LiCoO_2$, LCO) can be utilized as a thin-film type cathode due to its high theoretical energy density of 274 mA h g^{-1}, high working voltage of ~3.9 V, and excellent electrical conductivity.[9–13] Sputtering deposition, chemical vapor deposition, and e-beam evaporation methods have been used to fabricate LCO thin-film electrodes.[14–19] Among them, sputtering deposition methods with high process efficiency and excellent availability have been intensively studied.

Despite various merits of LCO, LCO cathode material has poor stability at high temperature with structural unstability during cycling at >4.2 V *vs.* Li/Li^+.[20–22] To overcome these disadvantages, LCO-based electrode structures partially exchanged with electrochemically active transition metals such Fe, Ti, and Ni instead of Co or doped with inactive materials such as Al and Mg have been proposed.[23–26] Furthermore, LCO electrode coated with metal oxides (Al_2O_3, ZrO_2, and TiO_2) has exhibited significantly improved LIB performance.[27–31] In particular, metal oxide coating on LCO electrodes can significantly enhance the stability of electrodes by protecting active materials due to HF generated by side reaction of $LiPF_6 + H_2O \rightarrow LiF + POF_3 + 2HF$.[32,33] Among these oxides, TiO_2 is a promising candidate for coating on LCO electrodes because of its low cost, non-toxicity, and stability.[34–36] In this study, we fabricated TiO_2-coated LCO electrodes using sputtering deposition method for LIBs. These TiO_2-coated LCO electrodes were evaluated and compared with LCO electrode without TiO_2.

2 Experimental

Fabrication of LCO–TiO_2 electrodes

LCO–TiO_2 electrodes as cathodes for lithium-ion batteries (LIBs) were fabricated using a radio-frequency (RF) magnetron sputtering deposition method on Al foil (Hohsen Corporation) as a substrate using $LiCoO_2$ (99.9% LTS chemical) and TiO_2 (99.9% LTS chemical) as sputtering targets. Prior to a main sputtering, a pre-sputtering was performed for 30 min to remove impurities on the target surface. The main sputtering process was carried out under a working pressure of 1.1×10^{-2} torr with an Ar gas flow rate of 30 standard cubic centimeter per min (sccm). First, LCO layers were deposited with an RF power of 80 W for 3 h. Then, TiO_2 layers were formed on the LCO electrode layers with an RF power of 10 W for 0, 60, 90, and 120 s (denoted as LCO–TiO_2(0), LCO–TiO_2(60), LCO–TiO_2(90), and LCO–TiO_2(120), respectively). For a homogeneous

Department of Chemical Engineering, Soongsil University, Seoul 06978, Republic of Korea. E-mail: kwpark@ssu.ac.kr; Fax: +82-2-812-5378; Tel: +82-2-820-0613

† Electronic supplementary information (ESI) available. See DOI: 10.1039/c8ra10451d

deposition, a substrate was rotated with a rotating speed of 3 rpm. These as-deposited electrodes were heated at 600 °C under an air atmosphere for 3 h. The loading amount of each electrode was about 0.13–0.16 mg cm^{-2}.

Structural characterization

To confirm the crystal structure of the as-formed electrodes, an X-ray diffractometer (XRD, D2 PHASER, Bruker AXS) was operated at a working voltage of 30 kV with a Cu K_α ($\lambda = 0.15418$ nm) and an Ni filter. The morphology and elemental distribution of the electrodes were characterized using a field emission scanning electron microscope (FE-SEM, GeminiSEM 300, ZEISS) operating at 2 kV.

Electrochemical measurement

To characterize the electrochemical properties of the electrodes, coin cells (size 2032, Hohsen corporation) were assembled using the sputtered samples as cathodes in an Ar-filled glove box (5 ppm, H_2O and O_2). Lithium foil (FMC Corporation) and porous polyethylene film were utilized as counter electrode and separator, respectively. Then, 1.1 M $LiPF_6$ (Soulbrain Co., Ltd.) in a mixture solution of ethylene carbonate : dimethyl carbonate (1 : 1) was used as electrolyte. Electrochemical analysis of the assembled coin cells was perfromed using a multichannel tester (WBCS300L, Wonatech Co.). Charge and discharge processes were carried out at 25 °C at a galvanostatic/potentiostatic and a galvanostatic modes, respectively, in the potential range of 3.01–4.30 V *vs.* Li/Li^+ for 100 cycles. High-rate performance of each sample was characterized at varying current densities from 0.1 to 1C. To evaluate the stability of the electrodes at a high potential, the charge–discharge process was performed in the potential range of 3.01–4.50 V *vs.* Li/Li^+ at a current density of 0.5C for 100 cycles. Cyclic voltammograms (CVs) of the electrodes were obtained by sweeping in the potential range of 3.01–4.30 V *vs.* Li/Li^+ at a scan rate of 0.1 mV s^{-1}.

3 Results and discussion

Fig. 1(a) and (c) show the XRD patterns of the electrodes formed on Al foils using a sputtering deposition method. Prior to a heating process, the as-deposited electrodes exhibited amorphous $LiCoO_2$ and TiO_2 phases with the XRD peaks related to an Al foil used as a substrate. To obtain high-crystalline structure of a $LiCoO_2$ cathode material, the electrodes were heated at 600 °C under an air atmosphere. Fig. 1(b) and (d) show the XRD patterns of the heated electrodes (LCO–TiO_2(0), LCO–TiO_2(60), LCO–TiO_2(90), and LCO–TiO_2(120)). The XRD peak at $2\theta = 19°$ corresponds to the (003) plane of $LiCoO_2$ layered structure.[37–39] On the other hand, no XRD peak related to TiO_2 phase appeared, demonstrating the formation of an amorphous TiO_2 on the $LiCoO_2$ crystalline structure. Fig. 2 shows SEM cross-sectional images of the as-prepared LCO–TiO_2(0), LCO–TiO_2(60), LCO–TiO_2(90), and LCO–TiO_2(120) electrodes. The thicknesses of LCO–TiO_2(0), LCO–TiO_2(60), LCO–TiO_2(90), and LCO–TiO_2(120) were 398, 402, 406, and 410 nm, respectively.

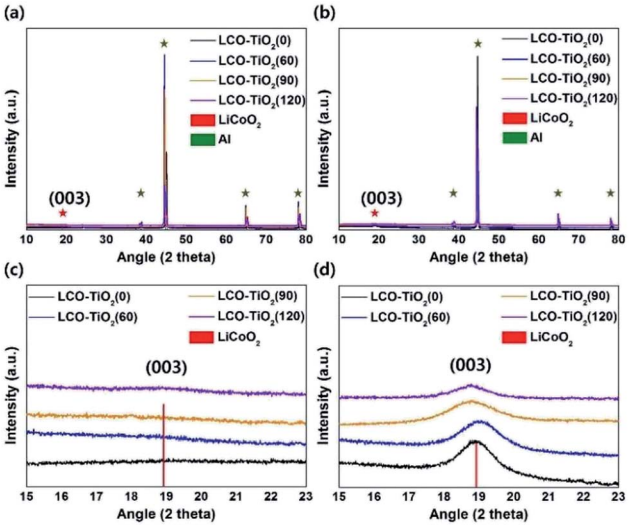

Fig. 1 XRD patterns of (a) the as-prepared and (b) heated LCO–TiO_2 electrodes. Enlarged XRD patterns to see the (003) plane of $LiCoO_2$ of (c) the as-prepared and (d) heated LCO–TiO_2 electrodes.

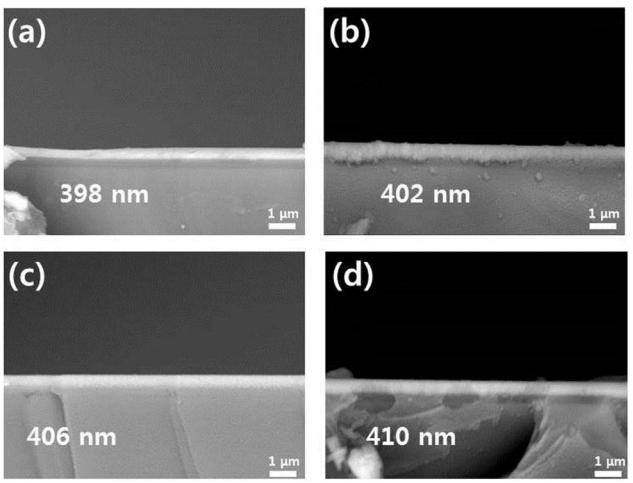

Fig. 2 (a) Cross-section SEM images of LCO–TiO_2(0), (b) LCO–TiO_2(60), (c) LCO–TiO_2(90), and (d) LCO–TiO_2(120).

With increasing deposition time of TiO_2 from 60 to 120 s, the film thickness increased from 402 to 410 nm due to the additional deposition of TiO_2 layer on the LCO electrode with a thickness of 398 nm (Fig. S1†). Thus, the thicknesses of the TiO_2 layers in LCO–TiO_2(60), LCO–TiO_2(90), and LCO–TiO_2(120) were 4, 8, and 12 nm, respectively.

Charge/discharge characteristic curves of LCO–TiO_2(0), LCO–TiO_2(60), LCO–TiO_2(90), and LCO–TiO_2(120) were obtained in the potential range of 0–4.3 V *vs.* Li/Li^+ with 0.5 C-rate for 100 cycles (Fig. 3(a) and S2†). LCO–TiO_2(0) exhibited an initial capacity of 80 mA h g^{-1} and a rapid capacity drop after 50 cycles. In contrast, LCO–TiO_2(60), LCO–TiO_2(90), and LCO–TiO_2(120) with TiO_2-coating layers showed relatively high capacities of 93, 103, and 107 mA h g^{-1}, respectively without serious capacity drop up to 100 cycles. The capacity retentions of LCO–TiO_2(0), LCO–TiO_2(60), LCO–TiO_2(90), and LCO–

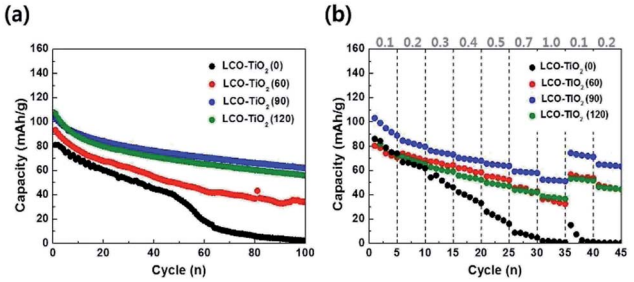

Fig. 3 (a) Comparison of cycling performance for the electrodes measured at 0.5C for 100 cycles in the potential range of 3.01–4.30 V *vs.* Li/Li$^+$. (b) High-rate performance of the electrodes measured with varying C-rates from 0.1 to 1.0 C.

TiO_2(120) were 2.5%, 26.6%, 60.2%, and 52.3%, respectively. Fig. 3(b) shows comparison of rate cycling performance of the electrodes measured with varying current densities from 0.1 to 1.0C. The average capacities of LCO–TiO_2(0) measured at 0.1, 0.2, 0.3, 0.4, 0.5, 0.7, and 1.0C, were 80, 65, 51, 37, 21, 7, and 1 mA h g^{-1}, respectively. To investigate recovery in capacity, the average capacities of LCO–TiO_2(0) measured at 0.1 and 0.2C were 6 and 0.4 mA h g^{-1}, respectively, demonstrating the damaged electrode due to fast cycling process. The average capacities of LCO–TiO_2(60) measured at 0.1, 0.2, 0.3, 0.4, 0.5, 0.7, and 1.0C, were 75, 71, 65, 60, 53, 44, and 34 mA h g^{-1}, respectively. The average capacities of LCO–TiO_2(90) measured at 0.1, 0.2, 0.3, 0.4, 0.5, 0.7, and 1.0C, were 95, 82, 75, 69, 64, 58, and 51 mA h g^{-1}, respectively. The average capacities of LCO–TiO_2(120) measured at 0.1, 0.2, 0.3, 0.4, 0.5, 0.7, and 1.0C, were 78, 68, 60, 54, 48, 42, and 37 mA h g^{-1}, respectively. Compared to LCO–TiO_2(0), the TiO_2-coated LCO electrodes showed high average capacities and improved recovery properties. Such enhanced electrochemical performance of the LCO electrodes containing amorphous TiO_2 layers with nanometer scale thickness may be attributed to fast ionic conductivity and low charge transfer resistance.[28,36,40]

Fig. 4(a)–(d) shows cyclic voltammograms (CVs) measured with a scan rate of 0.1 mV s^{-1} in the potential range of 3.0–4.3 V for LCO–TiO_2(0), LCO–TiO_2(60), LCO–TiO_2(90), and LCO–TiO_2(120), respectively. All these electrodes exhibited anodic and cathodic peaks at 3.86 and 3.92 V, respectively, associated with deinsertion reaction and insertion of Li$^+$ ions, respectively, in crystalline $LiCoO_2$ electrodes. In general, LCO electrodes heated at relatively low temperatures showed anodic and cathodic peaks at 3.64 and 3.75 V, respectively. Interestingly, another cathodic peaks corresponding to insertion of Li$^+$ ions in amorphous $LiCoO_2$ electrode appeared at 3.82 V.[39] Despite fairly high heating temperature of 600 °C, slight amorphous $LiCoO_2$ phases were found to be remained in these electrodes.

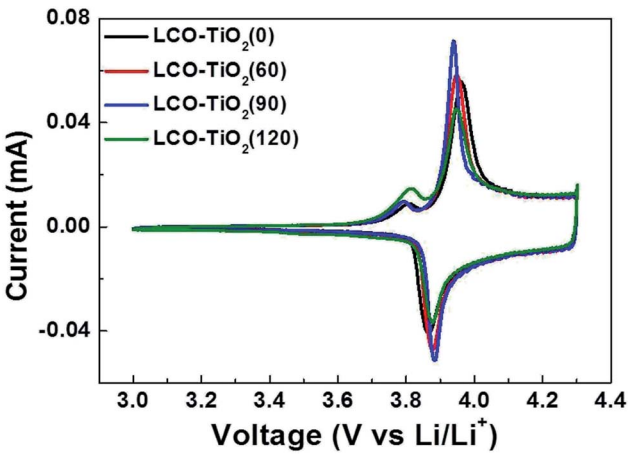

Fig. 4 Cyclic volatmmograms (CVs) for the electrodes measured at a scan rate of 0.1 mV s^{-1} in the potential range of 3.01–4.30 V *vs.* Li/Li$^+$.

Fig. 5 shows SEM surface images of the electrodes before and after 100 cycles in the potential range of 0–4.3 V *vs.* Li/Li$^+$ with 0.5 C. As shown in Fig. 5(a)–(d), the as-prepared LCO–TiO_2(0), LCO–TiO_2(60), LCO–TiO_2(90), and LCO–TiO_2(120) electrodes before cycling exhibited fairly homogeneous deposition of LCO and TiO_2. In addition, from EDX mapping images, all electrodes showed the well-dispersion of elements related to LCO and TiO_2 (Fig. S3†) and the increased TiO_2 content with increasing sputtering time of TiO_2 target (Table S1†). Fig. 5(e)–(h) and S4† show SEM surface and cross-sectional images of LCO–TiO_2(0), LCO–TiO_2(60), LCO–TiO_2(90), and LCO–TiO_2(120), respectively, after 100 cycles. LCO–TiO_2(0) exhibited the surface crack and increased thickness (~4.9 μm) of the film due to volume expansion of LCO during the cycling. LCO–TiO_2(60) with 4 nm TiO_2 layer also exhibited the surface crack and increased thickness (~2.9 μm). On the other hand, LCO–TiO_2(90) and LCO–TiO_2(120) after 100 cycles showed significantly less surface damage and thickness (1.4 and 1.6 μm, respectively). The structural stability of LCO–TiO_2(90) and LCO–TiO_2(120) during cycling might be due to inhibition of volumetric expansion of LCO having TiO_2 coating layer with proper thickness.

To further investigate the effect of TiO_2 layer on the LCO, as shown in Fig. 6, the charge/discharge characteristic curves of LCO–TiO_2(0) and LCO–TiO_2(90) were obtained in the potential range of 0–4.5 V with 0.5C-rate for 100 cycles. The initial capacities of LCO–TiO_2(0) and LCO–TiO_2(90) were 83 and 112 mA h g^{-1}, respectively. However, LCO–TiO_2(0) prepared without TiO_2 layer exhibited a drastic capacity drop after 10 cycles and no capacity after 70 cycles whereas LCO–TiO_2(90) with a TiO_2 coating layer (8 nm in thickness) exhibited a discharge capacity of 45 mA h g^{-1} after 100 cycles with a retention rate of 40.2%. The surface images of LCO–TiO_2(0) and LCO–TiO_2(90) after 100 cycles in the potential range of 0–4.5 V were shown in Fig. S5.† LCO–TiO_2(0) exhibited the serous surface damage such as the formation of holes (Fig. S5(a)†) whereas LCO–TiO_2(90) exhibited a fairly clean surface state after cycling up to 4.5 V (Fig. S5(b)†). The surface states of LCO–TiO_2(90) before and after cycling were characterized using XPS analysis (Fig. S6†). In the Ti2p spectra, the characteristic peaks corresponding to TiO_2 were observed before and after cycling. Furthermore, the Li1s spectra contained the characteristic peaks at 24.1 and 54.4 eV before cycling with an additional peak at 55.2 eV associated with LiF after cycling. In the O1s spectra, the peaks at 529.6 eV corresponding to $LiCoO_2$ lattice were maintained during cycling with additional peaks at 531–534 eV related to LiO_2 and Li_2CO_3. In general, the formation reaction of HF ($LiPF_6 + H_2O \rightarrow LiF + POF_3 + 2HF$) during charge/discharge

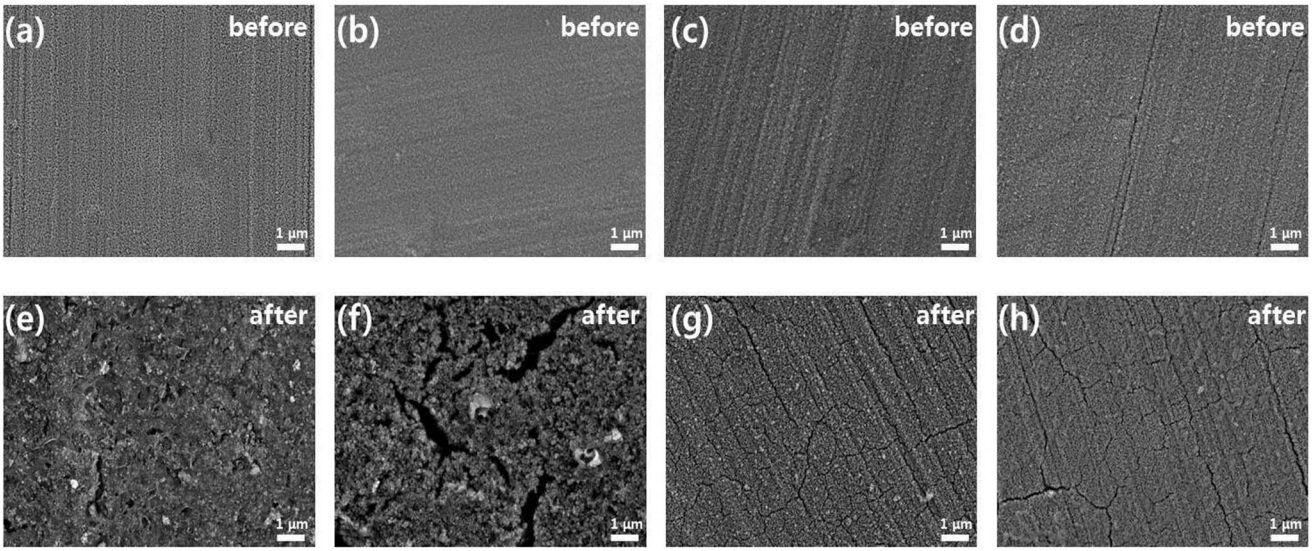

Fig. 5 SEM images of (a) and (e) LCO–TiO_2(0), (b) and (f) LCO–TiO_2(60), (c) and (g) LCO–TiO_2(90), and (d) and (h) LCO–TiO_2(120) before and after 100 cycles at a current density of 0.5C.

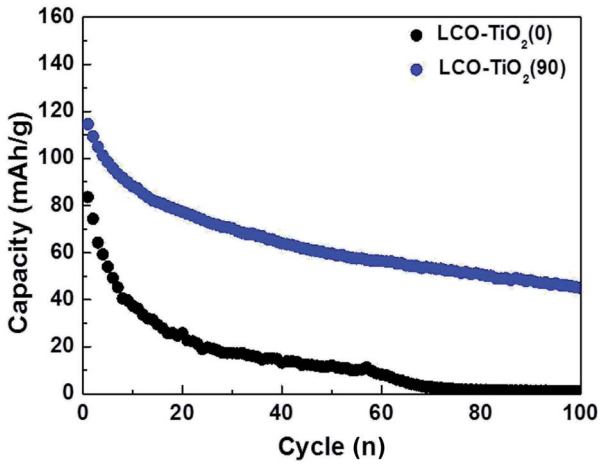

Fig. 6 Comparison of cycling performance for LCO–TiO_2(0) and LCO–TiO_2(90) measured at 0.5C for 100 cycles in the potential range of 3.01–4.50 V *vs.* Li/Li^+.

process can occur at a high electrode potential of >4.4 V.[29] The formed HF can lead to the deteriorated electrochemical performance of electrodes due to the damage of electrochemically active materials by HF.[41,42] However, the TiO_2 coating layer in LCO–TiO_2(90) can protect the LCO cathode from attacking by HF during the cycling, exhibiting improved electrochemical performance.

4 Conclusions

In summary, LCO electrodes in the absence and presence of TiO_2 layers as cathodes for LIBs were fabricated using sputtering deposition method. TiO_2 coating layers on the LCO electrodes were formed with varying TiO_2 sputtering time. Compared to LCO–TiO_2(0) prepared without TiO_2 coating layer, the TiO_2-coated LCO electrodes with proper layer thicknesses exhibited enhanced electrochemical performance, *i.e.* high capacity, improved retention, and high-rate cycling properties. The superior performance of the TiO_2-coated LCO electrodes was found to be attributed to the reduced volumetric expansion of LCO having TiO_2 coating layer with a proper thickness and the protection of the LCO electrodes against HF generated during cycling. Consequently, such TiO_2-coated LCO electrode can be used as a cathode candidate for high-performance thin-film LIBs.

Conflicts of interest

There are no conflicts to declare.

Acknowledgements

This research was supported by the Technology Development Program to Solve Climate Changes of the National Research Foundation (NRF) funded by the Ministry of Science, ICT (NRF-2017M1A2A2086648).

Notes and references

1 K. Kang, Y. S. Meng, J. Breger, C. P. Grey and G. Ceder, *Science*, 2014, **311**, 977–980.
2 J. M. Tarascon and M. Armand, *Nature*, 2001, **414**, 359–367.
3 J. B. Goodenough and K. S. Park, *J. Am. Chem. Soc.*, 2013, **135**, 1167–1176.
4 P. G. Bruce, B. Scrosati and J.-M. Tarascon, *Angew. Chem., Int. Ed.*, 2008, **47**, 2930–2946.
5 S. Kim, M. Kim, S. Han, G. Lee, H. Choe, D. Kwak, S. Choi, B. Son, M. Shin and K. Park, *Nano Energy*, 2016, **27**, 545–553.
6 Y. Wang, B. Liu, Q. Li, S. Cartmell, S. Ferrara, Z. D. Deng and J. Xiao, *J. Power Sources*, 2015, **286**, 330–345.

7 L. Xue, S. V. Savilov, V. V. Lunin and H. Xia, *Adv. Funct. Mater.*, 2018, **28**, 1–10.
8 S. Pat, S. Özen, H. H. Yudar, Ş. Korkmaz and Z. Pat, *J. Alloys Compd.*, 2017, **713**, 64–68.
9 R. Robert, C. Villevieille and P. Novák, *J. Mater. Chem. A*, 2014, **2**, 8589–8598.
10 S. Schuld, R. Hausbrand, M. Fingerle, W. Jaegermann and K. M. Weitzel, *Adv. Energy Mater.*, 2018, **8**, 1703411.
11 Z. Wang, Z. Wang, W. Peng, H. Guo, X. Li, J. Wang and A. Qi, *Ionics*, 2014, **20**, 1525–1534.
12 Q. Yang, J. Huang, Y. Li, Y. Wang, J. Qiu, J. Zhang, H. Yu, X. Yu, H. Li and L. Chen, *J. Power Sources*, 2018, **388**, 65–70.
13 G. Ting-Kuo Fey, C. Z. Lu, T. Prem Kumar and Y. C. Chang, *Surf. Coat. Technol.*, 2005, **199**, 22–31.
14 B. Wang, J. B. Bates, F. X. Hart, B. C. Sales, R. A. Zuhr and J. D. Robertson, *J. Electrochem. Soc.*, 1996, **143**, 3203–3213.
15 W. S. Yoon, S. H. Ban, K. K. Lee, K. B. Kim, M. G. Kim and J. M. Lee, *J. Power Sources*, 2001, **97–98**, 282–286.
16 J. S. Wook and S.-M. Lee, *J. Electrochem. Soc.*, 2007, **154**, A22–A25.
17 H. HakanYudar, S. Pat, S. Özen, R. Mohammadigharehbagh, C. Musaoğlu, Ş. Korkmaz and Z. Pat, *Vacuum*, 2018, **152**, 248–251.
18 J. B. Bates, N. J. Dudney, B. J. Neudecker, F. X. Hart, H. P. Jun and S. A. Hackney, *J. Electrochem. Soc.*, 2000, **147**, 59–70.
19 Z. Li, S. Yasui, S. Takeuchi, A. Creuziger, S. Maruyama, A. A. Herzing, I. Takeuchi and L. A. Bendersky, *Thin Solid Films*, 2016, **612**, 472–482.
20 Q. Liu, X. Su, D. Lei, Y. Qin, J. Wen, F. Guo, Y. A. Wu, Y. Rong, R. Kou, X. Xiao, F. Aguesse, J. Bareño, Y. Ren, W. Lu and Y. Li, *Nat. Energy*, 2018, **1–8**.
21 T. Zerrin, M. Ozkan and C. S. Ozkan, *MRS Adv.*, 2018, **3**, 3513–3518.
22 S. P. da Silva, L. E. Sita, C. S. dos Santos, F. H. Pavoni, H. de Santana, A. C. Andrello, P. R. C. da Silva and J. Scarminio, *Mater. Chem. Phys.*, 2018, **213**, 198–207.
23 S. Hu, C. Wang, L. Zhou, X. Zeng, L. Shao, J. Zhou, C. Zhou, C. Huang, X. Xi and L. Yang, *Ceram. Int.*, 2018, **44**, 14995–15000.
24 K. Sivajee Ganesh, B. Purusottam reddy, P. Jeevan Kumar and O. M. Hussain, *J. Electroanal. Chem.*, 2018, **828**, 71–79.
25 B. J. Kwon, P. J. Phillips, B. Key, F. Dogan, J. W. Freeland, C. Kim, R. F. Klie and J. Cabana, *Nanoscale*, 2018, **10**, 6954–6961.
26 Y. Gao and J. H. Li, *Adv. Mater. Res.*, 2012, **630**, 93–98.
27 D. Zuo, G. Tian, D. Chen and K. Shu, *Int. J. Electrochem. Sci.*, 2017, **12**, 5044–5057.
28 S. Tian, L. L. Liu, Y. S. Zhu, Y. Y. Hou, C. L. Hu and Y. P. Wu, *Funct. Mater. Lett.*, 2013, **6**, 10–13.
29 J. L. Tebbe, A. M. Holder and C. B. Musgrave, *ACS Appl. Mater. Interfaces*, 2015, **7**, 24265–24278.
30 J.-P. Noh, K.-T. Jung, M.-S. Jang, T.-H. Kwon, G.-B. Cho, K.-W. Kim and T.-H. Nam, *J. Nanosci. Nanotechnol.*, 2013, **13**, 7152–7154.
31 X. Li, J. Liu, X. Meng, Y. Tang, M. N. Banis, J. Yang, Y. Hu, R. Li, M. Cai and X. Sun, *J. Power Sources*, 2014, **247**, 57–69.
32 S. Yang, H. Qin, X. Li, H. Li and P. Yao, *J. Nanomater.*, 2017, **2017**, 1–10.
33 Y. Bi, T. Wang, M. Liu, R. Du, W. Yang, Z. Liu, Z. Peng, Y. Liu, D. Wang and X. Sun, *RSC Adv.*, 2016, **6**, 19233–19237.
34 S.-J. Kim, M.-C. Kim, D.-H. Kwak, D.-M. Kim, G.-H. Lee, H.-S. Choe and K.-W. Park, *J. Power Sources*, 2016, **304**, 119–127.
35 A. Zhou, Y. Lu, Q. Wang, J. Xu, W. Wang, X. Dai and J. Li, *J. Power Sources*, 2017, **346**, 24–30.
36 S. S. Jayasree, S. Nair and D. Santhanagopalan, *ChemistrySelect*, 2018, **3**, 2763–2766.
37 J.-P. Noh, G.-B. Cho, K.-T. Jung, W.-G. Kang, C.-W. Ha, H.-J. Ahn, J.-H. Ahn, T.-H. Nam and K.-W. Kim, *Mater. Res. Bull.*, 2012, **47**, 2823–2826.
38 H. Y. Park, S. C. Nam, Y. C. Lim, K. G. Choi, K. C. Lee, G. B. Park, H. P. Kim and S. B. Cho, *Korean J. Chem. Eng.*, 2006, **23**, 832–837.
39 J. P. Noh, K. T. Jung, G. B. Cho, S. H. Lee, K. W. Kim and T. H. Nam, *J. Nanosci. Nanotechnol.*, 2012, **12**, 5937–5941.
40 Y. Cho, J. Eom and J. Cho, *J. Electrochem. Soc.*, 2010, **157**, A617–A624.
41 Y. S. Jung, A. S. Cavanagh, A. C. Dillon, M. D. Groner, S. M. George and S. H. Lee, *J. Electrochem. Soc.*, 2010, **157**, A75–A81.
42 Y. Li, G. M. Veith, K. L. Browning, J. Chen, D. K. Hensley, M. P. Paranthaman, S. Dai and X. G. Sun, *Nano Energy*, 2017, **40**, 9–19.